remote sensing

MDPI

Article

Detection of Coral Reef Bleaching by Multitemporal Sentinel-2 Data Using the PU-Bagging Algorithm: A Feasibility Study at Lizard Island

Ke Wu [1,*], Fan Yang [1], Huize Liu [1] and Ying Xu [2,3]

[1] School of Geophysics and Geomatics, China University of Geosciences, Wuhan 430074, China; carpediem@cug.edu.cn (F.Y.); huizeliu@cug.edu.cn (H.L.)
[2] National Satellite Ocean Application Service, Ministry of Natural Resources, Beijing 100081, China; xuying@mail.nsoas.org.cn
[3] Key Laboratory of Space Ocean Remote Sensing and Application, Ministry of Natural Resources, Beijing 100081, China
* Correspondence: kewu@cug.edu.cn

Abstract: Coral reef bleaching events have become more frequent all over the world and pose a serious threat to coral reef ecosystems. Therefore, there is an urgent need for better detection of coral reef bleaching in a time- and cost-saving manner. In recent years, remote sensing technology has often been utilized and gained recognition for coral reef bleaching detection. However, bleaching corals in the water always have weak spectral change signals, causing difficulties in using remote sensing data. Additionally, uneven change samples make it challenging to adequately capture the details of coral reef bleaching detection and produce thematic maps. To resolve these problems, a novel method named coral reef bleaching detection by positive-unlabeled bagging (CBD-PUB) is proposed in this paper. To test the capacity of the method, a series of multi-temporal Sentinel-2 remote sensing images are utilized, and Lizard Island in Australia is taken as a case study area. The pseudo-invariant feature atmospheric correction (PIF) algorithm is adopted to improve coral reef bleaching spectral signals. After that, CBD-PUB is employed to effectively explore coral reef bleaching variation and its corresponding influence relations. The experimental results show that the overall accuracy of bleaching detection by the proposed algorithm reaches 92.1% and outperforms the traditional method. It fully demonstrates the feasibility of the model for the field of coral reef bleaching detection and provides assistance in the monitoring and protection of coral environments.

Keywords: coral reef bleaching; Sentinel-2; multitemporal; PU-bagging; Lizard Island

check for updates

Citation: Wu, K.; Yang, F.; Liu, H.; Xu, Y. Detection of Coral Reef Bleaching by Multitemporal Sentinel-2 Data Using the PU-Bagging Algorithm: A Feasibility Study at Lizard Island. *Remote Sens.* **2024**, *16*, 2473. https://doi.org/10.3390/rs16132473

Academic Editor: Dino Ienco

Received: 13 May 2024
Revised: 21 June 2024
Accepted: 28 June 2024
Published: 5 July 2024

Copyright: © 2024 by the authors. Licensee MDPI, Basel, Switzerland. This article is an open access article distributed under the terms and conditions of the Creative Commons Attribution (CC BY) license (https://creativecommons.org/licenses/by/4.0/).

1. Introduction

Coral reefs support immense biodiversity and provide important ecosystem services to many millions of people [1]. However, coral reefs are under significant threat of gradual degradation due to a combination of natural and man-made factors on a global scale [2,3]. Coral reefs are particularly vulnerable to ocean warming because they can tolerate only a very narrow temperature range. When the temperature exceeds the normal maximum temperature in summer by one degree Celsius, coral reefs undergo heat stress. One of the responses to severe heat stress is large-scale coral reef bleaching, and severe and long-term bleaching will cause substantial coral reef loss [4–6]. Remote sensing technology has been utilized to monitor coral reef bleaching, which has received increasing attention due to its unique advantages [7–10]. To date, most coral reef bleaching detection (CBD) studies have focused on a single temporal remote sensing image to detect coral reef bleaching. However, it is difficult to detect coral reef bleaching, mainly because of the sensors' low spatial resolution relative to the scale of reef heterogeneity. Moreover, a further complication

is that pixels containing other substrate features (e.g., sand) can have similar reflectance to bleached coral reef pixels [11,12]. As a result, bleaching coral is often confused with sand and other substrates in the extraction process, resulting in poor accuracy of the final extraction results.

Under these circumstances, some researchers have considered detecting coral reef bleaching using multi-temporal images [13,14]. It is based on significant changes in pixel brightness or color in images of the same location. When an abnormal increase in the digital number (DN) value of a coral occurs, coral reef bleaching is considered to have occurred [15,16]. In order to solve the radiometric differences between different scenes, the mutual correction method between multitemporal images is widely used for water column correction. The pseudo-invariant features (PIFs) correction technique is an empirical line conversion based on the assumption of a linear relationship between image bands across time for features that are spatially well-defined and spectrally radiometrically stable. After that, the differential images (DI) are compared to obtain the final change map. This method has been proven to have certain advantages in coral reef bleaching detection and has been receiving more attention due to its unique advantages under the condition that a large amount of measured data cannot be obtained. For example, Elvidge et al. provided a satisfactory account of multitemporal images using PIFs and DI-based approaches to detect coral reef bleaching in the Great Barrier Reef [9]. Rowlands et al. used the PIF algorithm based on multitemporal images to obtain information on bleaching corals on Roatan Island and analyzed the advantages of the algorithm for coral reef bleaching detection [10]. In particular, the spatial resolution of satellite data significantly impacts the accuracy of bleaching detection. That is, remote sensing data with high spatial resolution facilitate more accurate and detailed mapping of coral reef bleaching. As a result, some studies have focused on remote sensing data with high spatial resolution, such as images from commercial instruments like Quickbird and WorldView [17,18]. However, the limited scan range of the sensor and the high price lead to a limited application for CBD. By contrast, Sentinel-2 combines several advantages, such as spatial resolution, spectral resolution, revisit period, and cost of satellite data for coral reef monitoring [18]. It has a shorter revisit period of 5 days, which makes it more favorable for use in time series or change detection methods. Additionally, it has a blue band that may improve atmospheric correction and enable imaging of shallow waters of coral reefs, with a spatial resolution of 10 m. Recently, Xu et al. followed the same approach, achieved good results, and proved the advantages of multitemporal Sentinel-2 data in bleaching coral detection [18].

Although great progress has been made in research, there are still several problems in CBD with multi-temporal remote sensing images. First, the small bleaching changes are difficult to capture. Research has shown that the bleaching event lasts for only a few weeks, after which the reef either returns to its original color or dies and is covered by algae over a period of weeks [19]. Thus, the coral reef spectral properties may show a high variability due to the inevitable external conditions, such as scene geometry, water column, and atmospheric effects, etc. Meanwhile, the bleaching coral cannot be found using the optical satellite image with low temporal resolution [18]. These factors can increase the error in the extraction of bleaching corals, resulting in low accuracy of bleaching identification and a mismatch with reality. Next, valid prior knowledge of bleaching corals is always insufficient when bleaching coral identification is implemented based on remotely sensed imagery. Due to the difficulty of on-site data collection, in the real scenario, only a very small amount of data in the bleaching coral can be labeled. Suppose that 5% of the samples in the training set are labeled as bleaching corals while the rest of the samples are unlabeled. This can lead to a mismatch between recognition results and in situ data. Therefore, the sample imbalance problem distinguishes this task from traditional simple classification.

In view of this way of thinking, a novel algorithm named coral reef bleaching detection by positive-unlabeled bagging (CBD-PUB) is proposed in this paper. First, a large number of multitemporal Sentinel-2 images with short intervals are chosen to capture more detailed information about changes in coral reef bleaching. These images will be more conducive to reef monitoring due to their high temporal resolution. Second, all images are normalized by the PIF atmospheric correction approach to enhance the spectral change information of bleaching coral reefs. Since bleaching increases the coral reef reflectance value, the blue-green bands of each phase are multiplied to amplify this difference. All of the product bands are fused into a composite image. Thus, the spectral signatures of the multitemporal images are considered to be a stacked feature space. Third, a semi-supervised PU-bagging algorithm is proposed according to the small and unbalanced bleach coral samples. Different from traditional methods, it can obtain high-precision classification results in the case of only positive samples and unlabeled samples, which is particularly suitable for applications with a large amount of unlabeled data, and the algorithm runs quickly. With a much larger amount of unlabeled data than positive samples, the PU-bagging algorithm is potentially useful as a semi-supervised binary classification algorithm for detecting past bleaching events. To fully demonstrate the advantages of this proposed method, Lizard Island, Australia, is chosen as a typical region for studying coral reef bleaching. Understanding the impact of coral reef bleaching in this region has important practical significance because coral is such a significant component of marine ecosystems. The objective of the study is to evaluate the effectiveness of CBD-PUB through a case study and compare different change analysis methods for bleaching detection. The organization of this article is as follows. Section 2 describes the materials and methods, including the study site, satellite data, and ground truth data. Section 3 presents the proposed CBD-PUB model. Section 4 describes the experimental results and provides a discussion. Section 5 draws the conclusions of this work.

2. Study Area and Data

2.1. Study Site

Lizard Island is Australia's northernmost island beach resort and is the ultimate location for luxury getaways, amenities, and diving. It is located 150 miles north of Cairns and 57 miles northeast of the Cooktown coast (Figure 1). The island is surrounded by fringing reefs with over 350 species of hard coral that frame the intricate reef communities surrounding the island. There are large areas of sand and deep-water areas around the coral community, which together constitute the complex ecosystem of the island. Figure 1 describes the approximate location of Lizard Island and the RGB composite images of bands 4, 3, and 2 of the Sentinel-2A image. There has been a massive coral reef bleaching event in the global tropics [20], a global event triggered by climate change-induced disruption of sea surface temperatures, amplified by a strong El Niño in 2016 [21,22]. For Australia's Great Barrier Reef, this resulted in the worst coral reef bleaching on record in 2016, with 85% of the mortality occurring within a 600 km area between the tip of Cape York and the northern part of Lizard Island [21]. Severe bleaching and die-off also occurred at all shelf locations in the Lizard Island region. The findings indicate that 22% of corals on the reef were dead due to severe bleaching as of early June 2016, most of which were shallow-water coral (less than 10 m deep), which is the most diverse and productive coral and the coral that provides important reef habitat for reef users (e.g., tourism) [22].

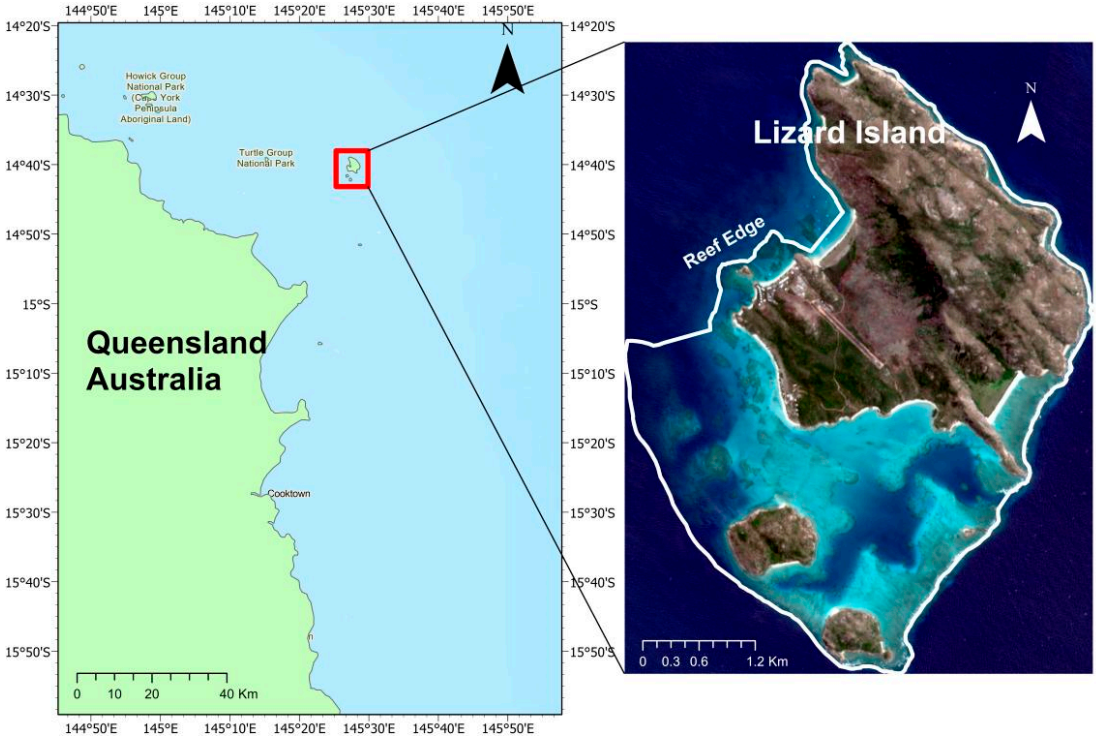


Figure 1. The general position of the Lizard Island and RGB composites of bands 4, 3, and 2 of Sentinel-2A image.

2.2. Satellite Data

Sentinel-2 includes the Copernicus Open Access Hub, which consists of Level-1C (L1C) and Level-2A (L2A) user products. The Sentinel-2 optical (https://scihub.copernicus.eu/, accessed on 23 January 2024) data were provided by the ESA through their open data policy. Sentinel-2 L1C user products undergo geographic projection, geometric correction, radiation correction, and resampling. On this basis, L2A user products undergo atmospheric correction, and the bottom-of-atmosphere reflectance for each band is ultimately obtained. Because the Open Access Hub does not provide L2A user products during the coral reef bleaching period in the study area, the L1C user products were utilized, and L1C data were transformed into L2 A-level data through the Sen2cor tool provided on the Open Access Hub. According to the time of the occurrence of the coral reef bleaching event in the Lizard Island region, 7 Sentinel-2 images from 24 November 2015 to 30 August 2016 were selected, as shown in Figure 2 Panel A–G. During the selection process, the cloud coverage over the coral area of Lizard Island is the most important indicator for selecting effective images. We have selected satellite images that are not covered by clouds in the coral area as much as possible.

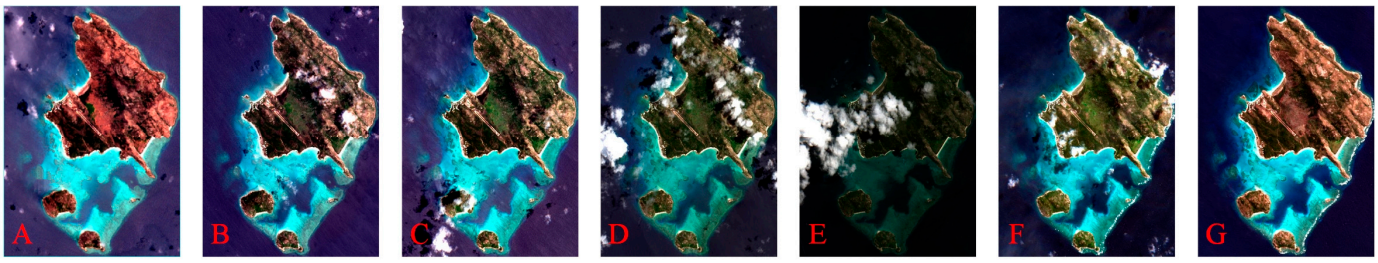


Figure 2. The original Sentinel-2 images from 12 November 2015 to 30 August 2016. (**A**–**G**) are images on 24 November 2015, 3 January 2016, 13 January 2016, 2 February 2016, 23 March 2016, 22 April 2016 and 30 August 2016, respectively.

2.3. Ground Truth

This study utilized the bleached coral data set published by Hoogenboom et al. at James Cook University [23,24]. It can be found in the final report that in the 2016 Great Barrier Reef coral reef bleaching event, the highest-risk period of large-scale bleaching in this study area was determined to be from early February to March 2016, which is the period with the greatest possibility of cumulative thermal stress exceeding the known bleaching threshold. The coral reef bleaching survey data were collected in the Lizard Island complex and its surrounding shoals, lagoons, and another middle shelf site in early March 2016. According to the report, a total of 6 sites were investigated, and 532 bleached Acropora corals were collected at a depth of no more than 6 m. In this survey, at the coral sites measured, the severity of bleaching ranged from 42% (minimum "white") to 99% (very close to pure white), and 71% of coral communities had whiteness values greater than 80. As shown in Figure 3, most of the sampling sites are located to the south of Lizard Island. We use the red points to represent bleaching coral sample points. Additionally, 40 sand points are selected through the visual interpretation and shown as yellow. In order to avoid scale problems, the bleaching coral vector points have been rasterized and must be the same size as the Sentinel-2 data. Panels A–F in Figure 3, respectively, represent the magnified distribution of bleaching coral sample points at different locations. It can be observed that the sample points at the same location have a high density and appear in the form of coral communities.

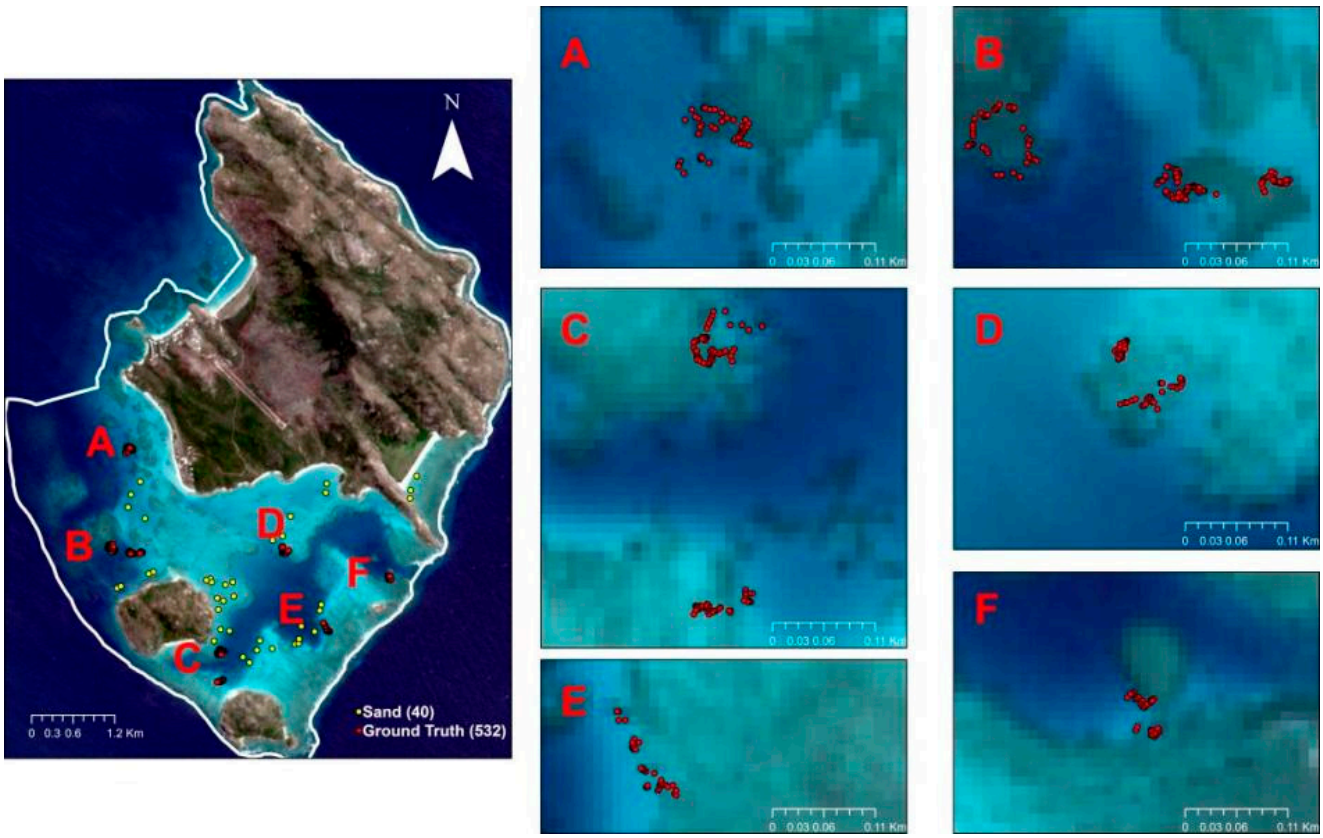


Figure 3. Map of bleaching coral and sands in the study area. Panels (**A**–**F**) are the local enlarged images of bleaching coral locations.

3. Methodology

The general scheme of the proposed CBD-PUB algorithm can be described as four steps, which are represented in Figure 4. These four steps are described in detail next.

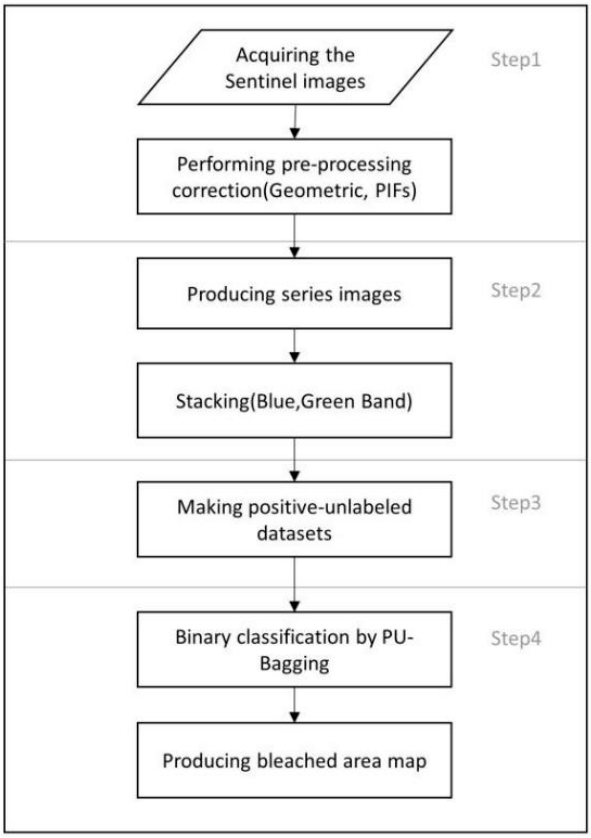


Figure 4. The overall workflow of the proposed CBD-PUB.

Step 1: Preprocessing of the multitemporal remote sensing images via the Sen2Cor tool is required. This tool performs atmospheric correction on L1C products and converts them into L2A products, and the bottom-of-atmosphere reflectance for each band is ultimately obtained. Then, changes in multitemporal images from different periods need to be detected; an inter-calibration is necessary in addition to the conventional spatial calibration. If the reflectance of the same invariant target shows differences between two dates, these differences might be largely caused by the water column effects. When the upper part of the study area covers the water column, the reflectance values of benthic organisms are imaged by the overlying water column, and this difference varies with the depth and wavelength of the light passing through the water [18,25,26]. Therefore, a water column correction algorithm needs to be selected to correct the image for coral reef bleaching detection. In this study, PIFs are used to normalize all multi-temporal images [27], as this algorithm is simple, fast, and does not require the acquisition of complex parameters, and the correction can be made just from the image itself. Finally, the bands of the remote sensing images used to detect coral reef bleaching events need to be determined, with a tendency to use only the blue and green bands for image interpretation due to the low permeability of the red band in water [9,28].

Step 2: A series of sequence images are generated and combined. The blue and green bands of each time phase were extracted separately. At the same time, to amplify the difference and increase the difference in the reflectance value of coral reef bleaching on the image, the blue-green bands of each phase are multiplied to produce a new band. All of the product bands are fused into a composite image. Each band of this composite image represents a temporal phase.

Step 3: The typical bleaching coral samples are extracted. The bleaching coral points are all marked as 1. The rest of the samples all have a value of 0, although they cannot be regarded as bleaching or not. At the same time, we set a "Hidden size" in the PU-bagging algorithm. "Hidden size" refers to the method of randomly selecting a specific number of

samples from the bleached coral reef samples (labeled as '1') and recategorizing them as '0'. These transformed samples are then hidden within the '0' labeled samples. The purpose of this process is to test the dependency of the CBD-PUB method on positive samples.

Step 4: The composite image is used as the training data, and the set of bleaching coral samples is used as a category label. The PU-bagging algorithm gives each pixel a score, and a higher score means that the pixel is more likely to be bleached. We take the average score of "Hidden size" as the threshold, and anything greater than the threshold can be regarded as bleached coral.

3.1. PIFs Algorithm

Assuming some pixels' values are constant in space and time, they can be regarded as PIF pixels, which can be regarded as crucial [9,10]. The images were corrected by fitting the relationship between PIF pixels in images of different phases. In order to describe the PIFs algorithm more directly, the diagram of the transform process is shown in Figure 5. As seen in Figure 5, the PIF pixels in the y-image are fitted to the PIF pixels in the x-image to obtain a linear equation containing a gain value a and an offset b. The image of either time phase is used as the reference image, and the images of the other time phases are normalized by the obtained linear equation (Equation (1)). The study can take the sand and deep ocean regions as light and dark pixels, respectively. At the same time, the first image is selected as the reference image x and the remaining temporal images as the image to be corrected y. The remaining temporal images y are normalized by the linear equation fitted to the light and dark pixels.

$$y = ax + b \tag{1}$$

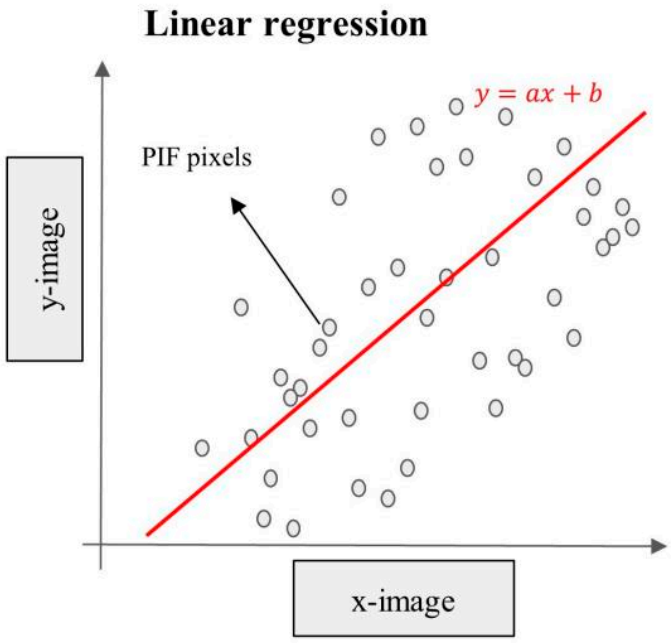


Figure 5. Diagram to obtain gain and offset values of PIFs.

3.2. PU-Bagging Algorithm

The PU-bagging algorithm sets the positive samples and unlabeled data as P and U, respectively, and gives a score of the similarity between image pixels and positive labels, which is proportional to the actual correct score [29]. It is trained on the basic assumption of completely random selection, which means that both P and U are used to obtain a standard classifier. Iterations are continuously performed by the classifier to find the positive sample with the highest probability in U [30]. After the iteration is completed, the classification results (0 or 1) obtained from the unmarked sample are accumulated, and the average score is obtained by dividing the accumulated value by the number of iterations. An unlabeled

sample is chosen if it has the highest average score [31,32], i.e., the sample has a high probability of bleaching. The PU-bagging algorithm can be described by the following steps: (1) Randomly select the same number (K) of unlabeled samples as the positive samples to form a "bootstrap" training set and construct a decision tree classifier; (2) Apply the classifier to the unlabeled samples in the different training sets "out of bag" and record their scores; (3) Iterate the above steps T times. Update the total score for each sample in the unlabeled data; (4) Calculate the average score $S(x)$ for each unlabeled sample.

$$S(x) = \frac{\sum_{t=1}^{T} f(x,t)}{T} = E(f(x,t)), t = 1, 2, \cdots T \quad (2)$$

The algorithm obtains scores in the range of 0 to 1. The closer the score of an unlabeled sample is to 1, the greater the similarity to the positive sample. After obtaining all the unlabeled sample scores, the mean scores of "Hidden sizes" were used as a threshold. When the score of the unlabeled sample was greater than this threshold, it was regarded as a positive sample. The pseudo-code can be described in Algorithm 1.

Algorithm 1. The pseudo-code of PU-bagging algorithm

Input: Unlabeled data, U
Positive samples, P
K = Number of the samples
T = Number of the iteration
Output: The score $S(x)$ of each x in U
initialization: $\forall\ x \in$ U, $n(x) \leftarrow 0$, $f(x,\ final) \leftarrow 0$, $S(x) \leftarrow 0$
for t = 1 to T do
Choose the sub-sample $\mathbf{U_t}$ with size K from U
Train the basic classifier $f(x,\ t)$ to discriminate P and U_t
For $x \in$ U$\backslash\mathbf{U_t}$, to update:
$f(x,\ final) \leftarrow f(x,\ final) + f(x,\ t)$
$n(x) \leftarrow n(x) + 1$
end for

3.3. Classifier

The classifier in the PU-bagging algorithm is the Classification and Regression Tree (CART), which is a technique for approximating the values of discrete functions with broad applicability to data [33]. The process of this classification algorithm is relatively simple. The core idea is to produce rules and a decision tree from sample data and then use the tree to analyze the unknown data. In this paper, CART is dichotomized using the Gini index. The purity of the dataset D can be measured by the Gini value:

$$\text{Gini}(D) = \sum_{k=1}^{n} \sum_{k' \neq k} p_k p_{k'} = 1 - \sum_{k=1}^{n} p_k^2 \quad (3)$$

where p_k is the probability of occurrence of category k and n is the number of categories. Intuitively, Gini(D) reflects the probability that two samples randomly selected from the dataset D will have inconsistent category labeling, so the smaller the Gini(D), the purer the dataset D is. In layman's terms, it can be understood that the Gini index is the probability that two samples are randomly drawn from the sample set with different categories. When the sample set is more impure, this probability is also larger; that is, the Gini index is also larger. From the above formula, it can be found that when there is only 1 class in the dataset D, p_k = 1 and Gini(D) = 0, indicating that the smaller the Gini index, the higher the sample purity.

For feature a, the set D is divided into D_1 and D_2. The Gini index is used to select the optimal dividing attribute, which is to compare the difference in the Gini indices of the different attributes after division and select the attribute that reduces the Gini index

of the sample set the most. Use the Gini index of the pre-division sample set D minus the weighted sum of the Gini indices of the post-division subsample set D^i.

$$\text{Gain}(D,a) = \text{Gini}(D) - \sum_{i=1}^{n} \frac{|D^i|}{|D|} \text{Gini}\left(D^i\right) \tag{4}$$

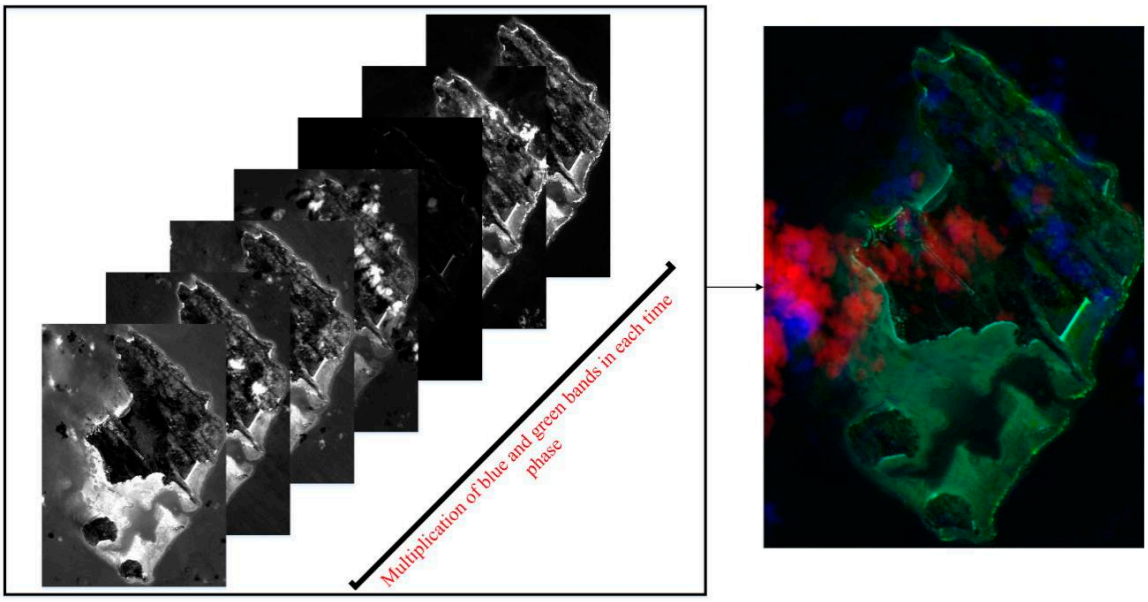
where $|D^i|$ denotes the number of samples in the dataset D^i. In the set of candidate attributes A, that attribute which makes the minimum Gini index after division is selected as the optimal division attribute, i.e.,

$$a^* = \text{argminGini } in \text{ ind}(D,a),\ a \in A \tag{5}$$

4. Results and Discussion

4.1. Bleaching Detection Results

The multi-temporal images were preprocessed and geo-corrected by the official Sentinel plugin Sen2Cor, using the first time phase image as the reference image and normalizing the rest of the images by the PIFs. Bleached coral reefs possess much higher reflectance in the blue-green band than healthy corals. Therefore, we extracted the blue and green bands of each image and multiplied them to obtain seven new bands, as shown in Figure 6a, which can be fused to obtain a new composite image in Figure 6b. In the new synthetic image, each band represents the product of one time phase blue and green band, so the spectral curve of this synthetic image represents the spectral time phase variation curve of the feature, and the study uses the time phase spectrum as a feature for the identification of bleached coral reefs.

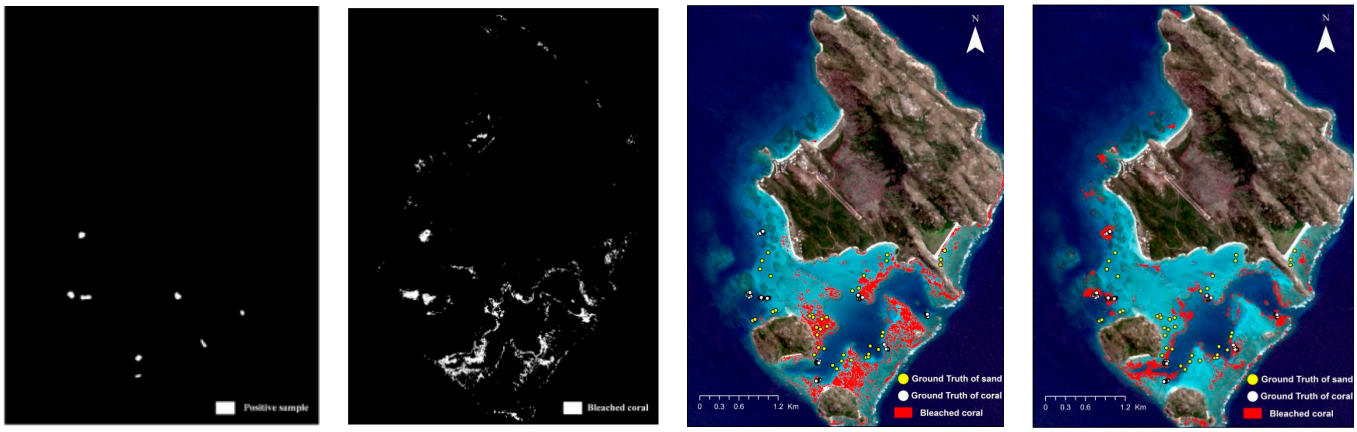


(**a**) (**b**)

Figure 6. The display of the composite image. (**a**) The blue and green bands in each time phase; (**b**) RGB composite image of the first three bands.

In order to implement the PU-bagging algorithm, a sample dataset needs to be generated first. The labels required for the experiments were generated from the publicly available bleaching dataset. All the bleached vector points in this bleached dataset were labeled as positive samples with a value of 1, generating a total of 532 whitened image pixels. In the whole whitened pixels, 70% were set as training data, and 30% were set as test data. A labeled image was produced, shown in Figure 7a, and fed into the PU-bagging algorithm. During the classification process, an equal number of positive and unlabeled

samples are randomly selected at a time to train the classifier, which is subsequently used to score the remaining image pixels in the image, and 1000 iterations are performed to obtain an average score for each image element. In the experiments, different "Hidden sizes" were tested, and finally, the average score of the "Hidden size" was used as a threshold (0.92). If the score is greater than this threshold, the corresponding pixel is considered a whitened reef and labeled as a white spot (Figure 7b), which can be superimposed on the remotely sensed image to generate a map of the coral reef bleaching results. In order to highlight the advantages of the CBD-PUB method, a DI-based approach is compared. The recognition results of the two methods are shown in Figure 7c,d, respectively. The yellow points are the ground truth of sand, the white points are the ground truth of coral, and the red points are the detected bleaching coral. From the visual comparison, it has been found that there are big differences between the two methods. DI can predict more bleaching corals in Figure 7c, but most of the bleaching areas are not correct. In contrast, the bleached coral reef result of CBD-PUB shows a more convincing image in Figure 7d.



(**a**) (**b**) (**c**) (**d**)

Figure 7. Result extracted by different algorithms. (**a**) The positive labeled samples. (**b**) The map of coral bleaching. (**c**) The result of the DI method. (**d**) The result of the CBD-PUB.

In addition, three typical areas (A, B, and C) are magnified and chosen for comparison in Figure 8a. Obviously, as shown in Figure 8b, there are large areas of missing bleached corals presented in A using the DI method. Meanwhile, lots of misjudgments can be found in B and C. It means the traditional algorithm cannot distinguish the bleached coral. Although CBD-PUB misclassifies the bleaching coral and sand, the result is better mainly because the position of the bleached coral can well be determined, as shown in Figure 8c.

The quantitative comparison results are shown in Table 1. Several evaluation indicators, including overall accuracy (OA), user's accuracy (UA), producer's accuracy (PA), and kappa coefficient (Kappa), are used to evaluate the proposed method exactly. In terms of OA, DI and CBD-PUB are 52.6% and 92.1%, respectively. The Kappa coefficient is consistent with accuracy. The advantage of the PU-bagging algorithm is strongly demonstrated in identifying the correct bleached coral reefs, with a high UA of 88.9%, whereas the DI only achieved 2.8%. Such results indicated that only a very small number of positive samples used in the proposed algorithm can correctly classify the bleached coral reefs. Although CBD-PUB misidentifies sand as albino coral, overall, it still has a significant advantage in identifying bleached coral reefs.

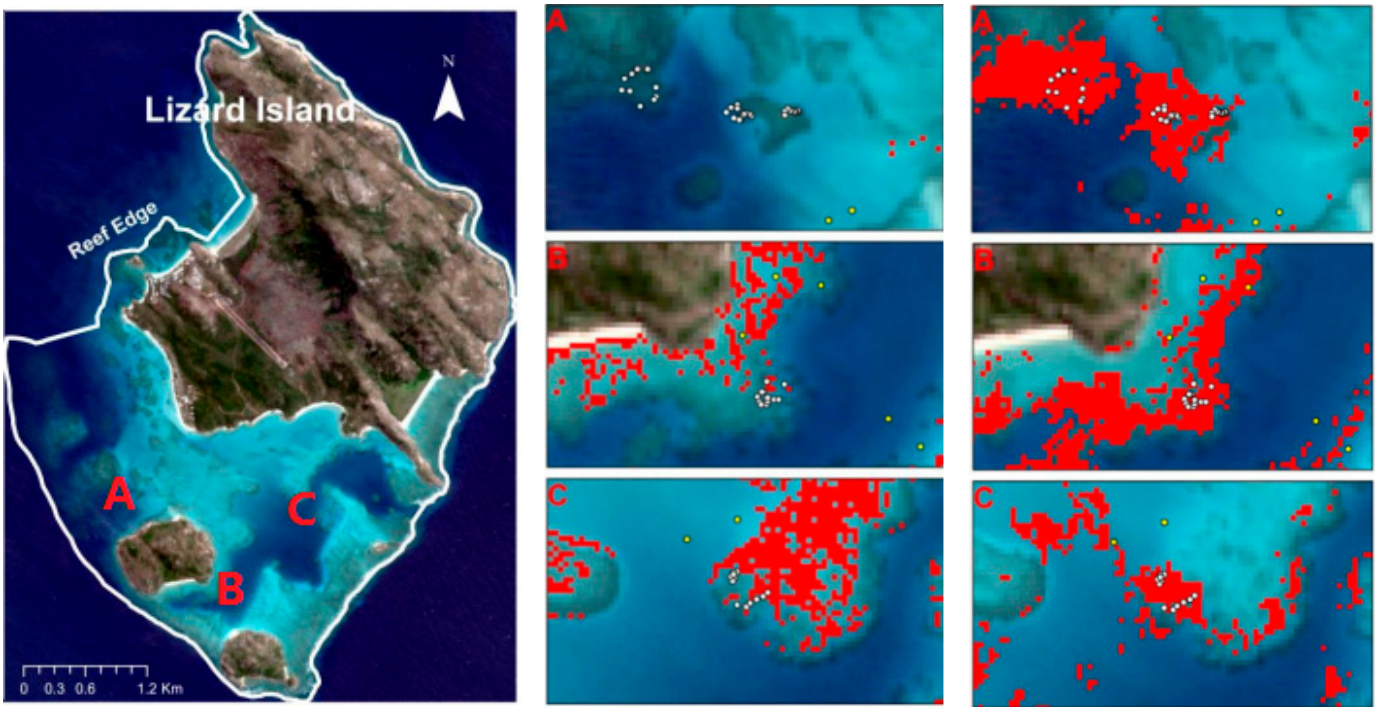


Figure 8. Three typical enlarged bleaching maps based on two algorithms. (**a**) Panels A, B, and C in the study area. (**b**) The result of the DI method. (**c**) The result of the CBD-PUB.

Table 1. Comparison of results of different methods.

Class	DI		Proposed	
	PA (%)	UA (%)	PA (%)	UA (%)
Bleached coral reefs	50	2.8	94.1	88.9
Sand	52.7	97.5	90.5	95
OA (%)	52.6		92.1	
Kappa	0.523		0.92	

4.2. The Effect of PIFs

To further illustrate the significance of the PIFs algorithm in this research, raw spectral curves of typical substrate types were compared with PIFs-corrected ones. For convenience, four points in the study area, representing different types, were selected.

As shown in Figure 9a, there are 1 sand point, 1 deep point, and 2 bleached coral points, which were randomly selected from the study site. Their spectra without PIFs and with PIFs are shown in Figure 9b. The x-axis is the time series from 12 November 2015 to 30 August 2016, and the y-axis is the spectral value. As shown in Figure 9b, the image DN values of the three cover types show different changes. Among them, the DN value of the light and dark pixels does not vary greatly (sand and deep water). In contrast, the DN value of coral has changed considerably. Before correction, the DN value of a large number of corals decreased significantly on 26 March, which is contrary to the occurrence of bleaching. This is due to the cloud shadows caused by the large number of clouds in this time phased image covering a large number of pixel points, resulting in a darker image and an overall decrease in DN values. The spectra of these points have a large difference after PIF correction in Figure 9b. The spectral values of the bleached corals increased significantly in March. It has been proven that the PIFs algorithm has improved the spectral information of multitemporal bleached corals. In summary, the corrected coral curve rises first and then decreases, which is consistent with the situation in which the DN value rises

after bleaching and then decreases after death or recovery. It provides more features for bleached coral monitoring.

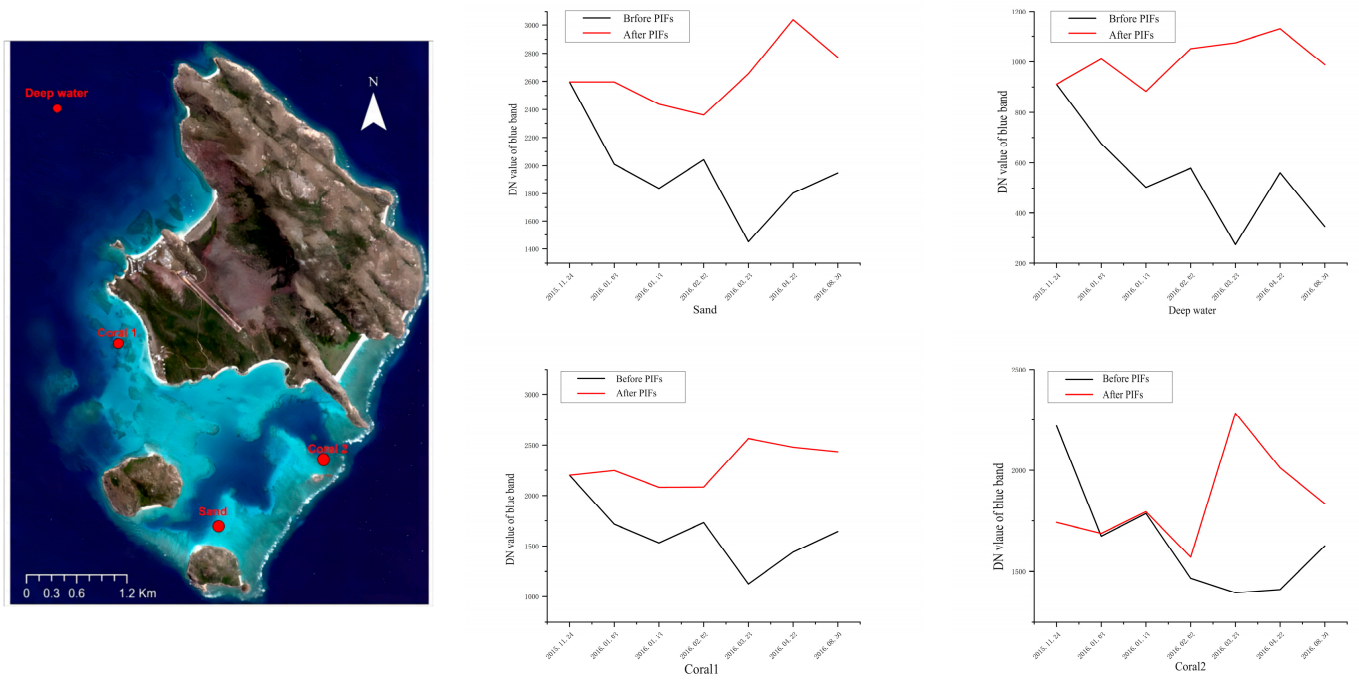


Figure 9. The effect of PIFs. (**a**) Randomly selected bleached corals, sand, and deep water. (**b**) Comparison between the spectral value with and without PIF correction.

4.3. Applicability of PU-Bagging

In this section, the average score of hidden positive samples in the PU-bagging model is used as the evaluation standard to detect the dependence of positive samples. When the number of hidden positive samples increases, the average score of the hidden samples will change and affect the algorithm. In the experiment, we kept increasing the "Hidden size" from 20 to 80. Figure 10 illustrates that the average score and accuracy increased with the increase in the number of hidden positive samples. The larger the "Hidden size" is, the smaller the number of positive samples used for training. When the "Hidden size" is 20, the positive samples are suitable for the model, and the score is the highest at 0.8782. Therefore, thresholds can be set according to this score, and bleaching coral detection accuracy is the highest at 0.921. As the "Hidden size" increases, the average score of "Hidden size" decreases from 0.8782 to 0.8288, but the decline is very small. Meanwhile, the accuracy decreases from 0.921 to 0.887. The above results show that the algorithm has little dependence on samples and can still maintain good detection results even when the number of positive samples is continuously reduced. It not only demonstrates the superiority of the PU-bagging algorithm in the field of bleaching detection but also provides a new idea for coral reef bleaching detection. Although the bleaching coral dataset has problems such as small sample size and unbalanced samples, the PUL algorithm can be improved to continuously improve the bleaching detection accuracy, making the results of bleaching coral detection by remote sensing technology more accurate and credible.

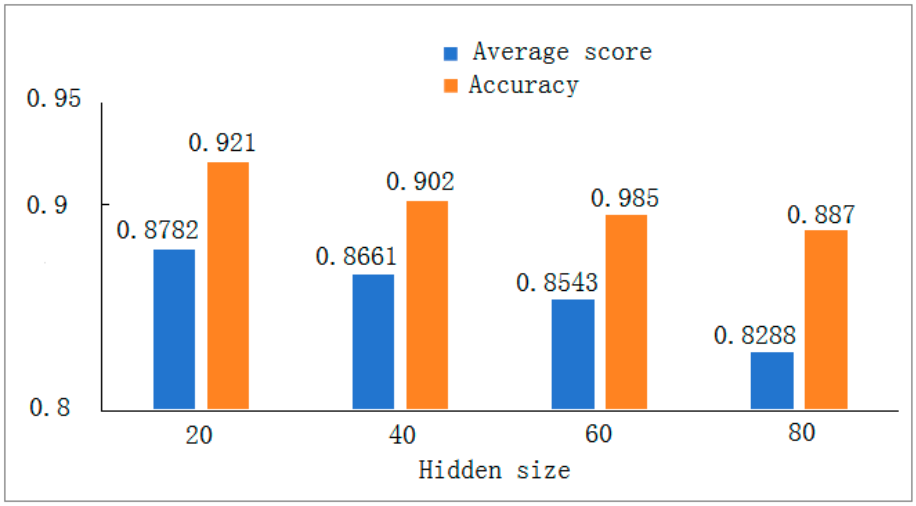


Figure 10. Effect of different numbers of positive samples on the PU-bagging algorithm.

5. Conclusions

In this study, a novel coral reef bleaching detection model, CBD-PUB, is proposed. The feasibility of the model of coral reef bleaching detection on Lizard Island, Australia, is demonstrated. In the model, a large number of Sentinel-2 datasets with different times were utilized to detect coral reef bleaching. It has been proven that remote sensing images with high revisit cycles can solve the problem that coral reef bleaching cycles are short and difficult to monitor. In addition, to amplify the spectral difference between the bleaching coral and others, the PIFs algorithm was adopted. The blue and green bands of each time phase are multiplied to produce new bands. All bands are fused to create a composite image, which greatly increases the change in information from bleaching coral. It can bring obvious changes to spectral analysis and lead to further improvements in the accuracy of coral reef bleaching detection. Finally, a semi-supervised machine learning algorithm (PU-bagging) solves the problem of coral sample imbalance to a great extent. Due to the scarcity of in situ bleaching data, there are only a small number of samples to train and test the model. Nevertheless, the semi-supervised machine learning approach can still obtain more accurate bleached areas compared with the traditional method. In the future, some new methods, such as deep learning, are recommended to be utilized in CBD applications. Change analysis based on remote sensing images is suggested to incorporate other marine environmental information, such as sea surface temperature, wave exposure, and ocean color, to detect and forecast bleaching.

Author Contributions: Conceptualization, K.W.; methodology, K.W. and F.Y.; software, F.Y.; formal analysis, K.W., H.L. and Y.X.; writing—original draft preparation, K.W. and F.Y.; writing—review and editing, K.W., H.L. and Y.X.; funding acquisition, K.W. All authors have read and agreed to the published version of the manuscript.

Funding: This research was funded by the National Natural Science Foundation of China, grant number U21A2013; the Open Fund of Wenzhou Future City Research Institute, grant number WL2023007; the Foundation of State Key Laboratory of Public Big Data, grant number PBD2023-28; the State Key Laboratory of Applied Optics, grant number SKLAO2021001A01; the Hebei Key Laboratory of Ocean Dynamics, Resources and Environments, grant number HBHY2302; the S & T Program of Hebei, grant number 21373301D; the Open Fund of State Key Laboratory of Remote Sensing Science, grant number OFSLRSS202312; the Fundamental Research Funds for the Central Universities, China University of Geosciences (Wuhan), grant number 2642022009; the Global Change and Air–Sea Interaction II under Grant, grant number GASI-01-DLYG-WIND0; the Open Fund of Key Laboratory of Space Ocean Remote Sensing and Application, MNR, grant number 202401001; the Open Fund of Key Laboratory of Regional Development and Environmental Response, grant number 2023(A)003.

Institutional Review Board Statement: Not applicable.

Informed Consent Statement: Not applicable.

Data Availability Statement: Coral reef bleaching data were derived from the following resources available in the public domain: [Acropora bleaching data, Lizard Island 2016, and https://doi.org/10.4225/28/591abebf0e781, accessed on 25 January 2024].

Acknowledgments: The authors would like to thank the editors and anonymous reviewers for their insightful comments and suggestions that led to this improved version and clearer presentation of the technical content.

Conflicts of Interest: The authors declare no conflicts of interest.

References

1. Hughes, T.P.; Barnes, M.L.; Bellwood, D.R.; Cinner, J.E.; Cumming, G.S.; Jackson, J.B.C.; Kleypas, J.; van de Leemput, I.A.; Lough, J.M.; Morrison, T.H.; et al. Coral Reefs in the Anthropocene. *Nature* **2017**, *546*, 82–90. [CrossRef] [PubMed]
2. Wilkinson, C. *Status of Coral Reefs of the World: 2008*; Global Coral Reef Monitoring Network and Reef and Rainforest Research Center: Townsville, Australia, 2008.
3. Gardner, T.A.; Côté, I.M.; Gill, J.A.; Grant, A.; Watkinson, A.R. Long-Term Region-Wide Declines in Caribbean Corals. *Science* **2003**, *301*, 958–960. [CrossRef]
4. Hoegh-Guldberg, O. Climate Change, Coral Bleaching and the Future of the World's Coral Reefs. *Mar. Freshw. Res.* **1999**, *50*, 839–866. [CrossRef]
5. Hughes, T.P.; Baird, A.H.; Bellwood, D.R.; Card, M.; Connolly, S.R.; Folke, C.; Grosberg, R.; Hoegh-Guldberg, O.; Jackson, J.B.C.; Kleypas, J.; et al. Climate Change, Human Impacts, and the Resilience of Coral Reefs. *Science* **2003**, *301*, 929–933. [CrossRef] [PubMed]
6. Hoegh-Guldberg, O.; Mumby, P.J.; Hooten, A.J.; Steneck, R.S.; Greenfield, P.; Gomez, E.; Harvell, C.D.; Sale, P.F.; Edwards, A.J.; Caldeira, K.; et al. Coral Reefs Under Rapid Climate Change and Ocean Acidification. *Science* **2007**, *318*, 1737–1742. [CrossRef] [PubMed]
7. Mumby, P.J.; Green, E.P.; Edwards, A.J.; Clark, C.D. The Cost-Effectiveness of Remote Sensing for Tropical Coastal Resources Assessment and Management. *J. Environ. Manag.* **1999**, *55*, 157–166. [CrossRef]
8. Clark, C.D.; Mumby, P.J.; Chisholm, J.R.M.; Jaubert, J.; Andrefouet, S. Spectral Discrimination of Coral Mortality States Following a Severe Bleaching Event. *Int. J. Remote Sens.* **2000**, *21*, 2321–2327. [CrossRef]
9. Elvidge, C.D.; Dietz, J.B.; Berkelmans, R.; Andréfouët, S.; Skirving, W.; Strong, A.E.; Tuttle, B.T. Satellite Observation of Keppel Islands (Great Barrier Reef) 2002 Coral Bleaching Using IKONOS Data. *Coral Reefs* **2004**, *23*, 123–132. [CrossRef]
10. Rowlands, G.P.; Purkis, S.J.; Riegl, B.M. The 2005 Coral-bleaching Event Roatan (Honduras): Use of Pseudoinvariant Features (PIFs) in Satellite Assessments. *J. Spat. Sci.* **2008**, *53*, 99–112. [CrossRef]
11. Hochberg, E.; Atkinson, M. Spectral Discrimination of Coral Reef Benthic Communities. *Coral Reefs* **2000**, *19*, 164–171. [CrossRef]
12. Hochberg, E.J.; Atkinson, M.J.; Andréfouët, S. Spectral Reflectance of Coral Reef Bottom-Types Worldwide and Implications for Coral Reef Remote Sensing. *Remote Sens. Environ.* **2003**, *85*, 159–173. [CrossRef]
13. Andréfouët, S.; Mumby, P.; McField, M.; Hu, C.; Muller-Karger, F. Revisiting Coral Reef Connectivity. *Coral Reefs* **2002**, *21*, 43–48. [CrossRef]
14. Palandro, D.; Andréfouët, S.; Dustan, P.; Muller-Karger, F.E. Change Detection in Coral Reef Communities Using Ikonos Satellite Sensor Imagery and Historic Aerial Photographs. *Int. J. Remote Sens.* **2003**, *24*, 873–878. [CrossRef]
15. Holden, H.; LeDrew, E. Spectral Discrimination of Healthy and Non-Healthy Corals Based on Cluster Analysis, Principal Components Analysis, and Derivative Spectroscopy. *Remote Sens. Environ.* **1998**, *65*, 217–224. [CrossRef]
16. Hedley, J.D.; Roelfsema, C.M.; Chollett, I.; Harborne, A.R.; Heron, S.F.; Weeks, S.; Skirving, W.J.; Strong, A.E.; Eakin, C.M.; Christensen, T.R.L.; et al. Remote Sensing of Coral Reefs for Monitoring and Management: A Review. *Remote Sens.* **2016**, *8*, 118. [CrossRef]
17. Kabiri, K.; Pradhan, B.; Shafri, H.Z.M.; Mansor, S.B.; Samimi-Namin, K. A Novel Approach to Estimate Diffuse Attenuation Coefficients for QuickBird Satellite Images: A Case Study at Kish Island, the Persian Gulf. *J. Indian Soc. Remote Sens.* **2013**, *41*, 797–806. [CrossRef]
18. Xu, J.; Zhao, J.; Wang, F.; Chen, Y.; Lee, Z. Detection of Coral Reef Bleaching Based on Sentinel-2 Multi-Temporal Imagery: Simulation and Case Study. *Front. Mar. Sci.* **2021**, *8*, 584263. [CrossRef]
19. Douglas, A.E. Coral Bleaching—-How and Why? *Mar. Pollut. Bull.* **2003**, *46*, 385–392. [CrossRef]
20. Hughes, T.P.; Kerry, J.T.; Álvarez-Noriega, M.; Álvarez-Romero, J.G.; Anderson, K.D.; Baird, A.H.; Babcock, R.C.; Beger, M.; Bellwood, D.R.; Berkelmans, R.; et al. Global Warming and Recurrent Mass Bleaching of Corals. *Nature* **2017**, *543*, 373–377. [CrossRef]
21. Hughes, T.P.; Anderson, K.D.; Connolly, S.R.; Heron, S.F.; Kerry, J.T.; Lough, J.M.; Baird, A.H.; Baum, J.K.; Berumen, M.L.; Bridge, T.C.; et al. Spatial and Temporal Patterns of Mass Bleaching of Corals in the Anthropocene. *Science* **2018**, *359*, 80–83. [CrossRef]
22. Great Barrier Reef Marine Park Authority. *2016 Coral Bleaching Event on the Great Barrier Reef*; Great Barrier Reef Marine Park Authority: Townsville, Australia, 2017.

23. Critchell, K.; Hoogenboom, M. *Acropora Bleaching Data, Lizard Island*; James Cook University: Cairns, Australia, 2016. [CrossRef]
24. Hoogenboom, M.O.; Frank, G.E.; Chase, T.J.; Jurriaans, S.; Álvarez-Noriega, M.; Peterson, K.; Critchell, K.; Berry, K.L.E.; Nicolet, K.J.; Ramsby, B.; et al. Environmental Drivers of Variation in Bleaching Severity of Acropora Species during an Extreme Thermal Anomaly. *Front. Mar. Sci.* **2017**, *4*, 376. [CrossRef]
25. Lyzenga, D.R. Passive Remote Sensing Techniques for Mapping Water Depth and Bottom Features. *Appl. Opt.* **1978**, *17*, 379–383. [CrossRef] [PubMed]
26. Lyzenga, D.R. Remote Sensing of Bottom Reflectance and Water Attenuation Parameters in Shallow Water Using Aircraft and Landsat Data. *Int. J. Remote Sens.* **1981**, *2*, 71–82. [CrossRef]
27. Schott, J.R.; Salvaggio, C.; Volchok, W.J. Radiometric Scene Normalization Using Pseudoinvariant Features. *Remote Sens. Environ.* **1988**, *26*, 1–16. [CrossRef]
28. Mishra, D.R.; Narumalani, S.; Rundquist, D.; Lawson, M. Characterizing the Vertical Diffuse Attenuation Coefficient for Downwelling Irradiance in Coastal Waters: Implications for Water Penetration by High Resolution Satellite Data. *ISPRS J. Photogramm. Remote Sens.* **2005**, *60*, 48–64. [CrossRef]
29. Elkan, C.; Noto, K. Learning Classifiers from Only Positive and Unlabeled Data. In Proceedings of the 14th ACM SIGKDD International Conference on Knowledge Discovery and Data Mining, New York, NY, USA, 24–27 August 2008; Association for Computing Machinery: New York, NY, USA, 2008; pp. 213–220.
30. Mordelet, F.; Vert, J.-P. A Bagging SVM to Learn from Positive and Unlabeled Examples. *Pattern Recognit. Lett.* **2014**, *37*, 201–209. [CrossRef]
31. Bekker, J.; Davis, J. Learning from Positive and Unlabeled Data: A Survey. *Mach Learn* **2020**, *109*, 719–760. [CrossRef]
32. Wu, B.; Qiu, W.; Jia, J.; Liu, N. Landslide Susceptibility Modeling Using Bagging-Based Positive-Unlabeled Learning. *IEEE Geosci. Remote Sens. Lett.* **2021**, *18*, 766–770. [CrossRef]
33. Xu, M.; Watanachaturaporn, P.; Varshney, P.K.; Arora, M.K. Decision Tree Regression for Soft Classification of Remote Sensing Data. *Remote Sens. Environ.* **2005**, *97*, 322–336. [CrossRef]

Disclaimer/Publisher's Note: The statements, opinions and data contained in all publications are solely those of the individual author(s) and contributor(s) and not of MDPI and/or the editor(s). MDPI and/or the editor(s) disclaim responsibility for any injury to people or property resulting from any ideas, methods, instructions or products referred to in the content.